ELECTRONIC AND MECHANICAL PROPERTIES OF CARBON NANOTUBES

L. Forró[1], J.-P. Salvetat[1], J.-M. Bonard[1], R. Bacsa[1], N.H. Thomson[1], S. Garaj[1], L. Thien-Nga[1], R. Gaál[1], A. Kulik[1], B. Ruzicka[2], L. Degiorgi[2], A. Bachtold[3], C. Schönenberger[3], S. Pekker[4], K. Hernadi[5]

[1]Département de Physique, EPF-Lausanne, CH-1015 Lausanne, Switzerland

[2]Laboratorium für Festkörperphysik, ETH-Zürich, CH-8093 Zürich, Switzerland

[3]Institut für Physik, Universität Basel, Klingelbergstr. 82, CH-4056 Basel, Switzerland

[4]Research Institute for Solid State Physics and Optics, H-1525 Budapest, Hungary

[5]Applied and Environmental Chemistry Department, JATE, H-6720 Szeged, Hungary

INTRODUCTION

Interest in carbon nanotubes has grown at a very rapid rate because of their many exceptional properties, which span the spectrum from mechanical and chemical robustness to novel electronic transport properties. Their physics, chemistry and perspectives for applications are very challenging. Below we highlight the main results of the Lausanne group and their collaborators on transport, electron spin resonance, elastic and field emission properties of single wall (SWNT) and multi-wall (MWNT) carbon nanotubes.

SAMPLES

We use MWNTs produced by arc discharge or by thermal decomposition of hydrocarbons, and SWNTs either prepared by the arc discharge method in the presence of catalysts or commercially available (Carbolex, Rice University, MER, DEL). The first step in the study of CNTs is technological: their purification. This is especially true for SWNTs, which are severely contaminated with magnetic catalyst particles. The purity of the arc-discharge fabricated MWNTs is much better, since magnetic materials are not used in their

production. Nevertheless they have to be separated from graphitic flakes, polyhedral particles and amorphous carbon present in the raw soot. For MWNTs, we have developed a soft purification method, which uses the properties of colloidal suspensions[1]. We started the purification with a suspension prepared from 500 ml of distilled water, 2.5 g of SDS (sodium dodecyl sulfate; a common surfactant) and 50 mg of MWNT arc powder sonicated for 15 minutes. Sedimentation and centrifugation (at 5000 rpm for 10 minutes) removed all graphitic particles larger than 500 nm from the solution, as confirmed by low magnification SEM observations (upper part of Fig. 1). We then added surfactant to the solution to reach 12 CMC (critical micelle concentration). At these surfactant concentrations, micelles form and induce flocculation, i.e. the formation of aggregates. These aggregates mostly contain large objects, while smaller objects remain dispersed, and sediment after a certain time, typically a few days. After decanting the suspension one week later, we repeat the procedure once or twice. Fig. 1 (lower part) shows scanning electron microscopy images of a MWNT deposit after the separation procedure. The untreated material contains a large proportion of nanoparticles (typically 70 % in number and 40 % in weight). After the purification, the material remaining in suspension consisted nearly exclusively of nanoparticles, while the sediment contained nanotubes with a content of over 80 % in weight.

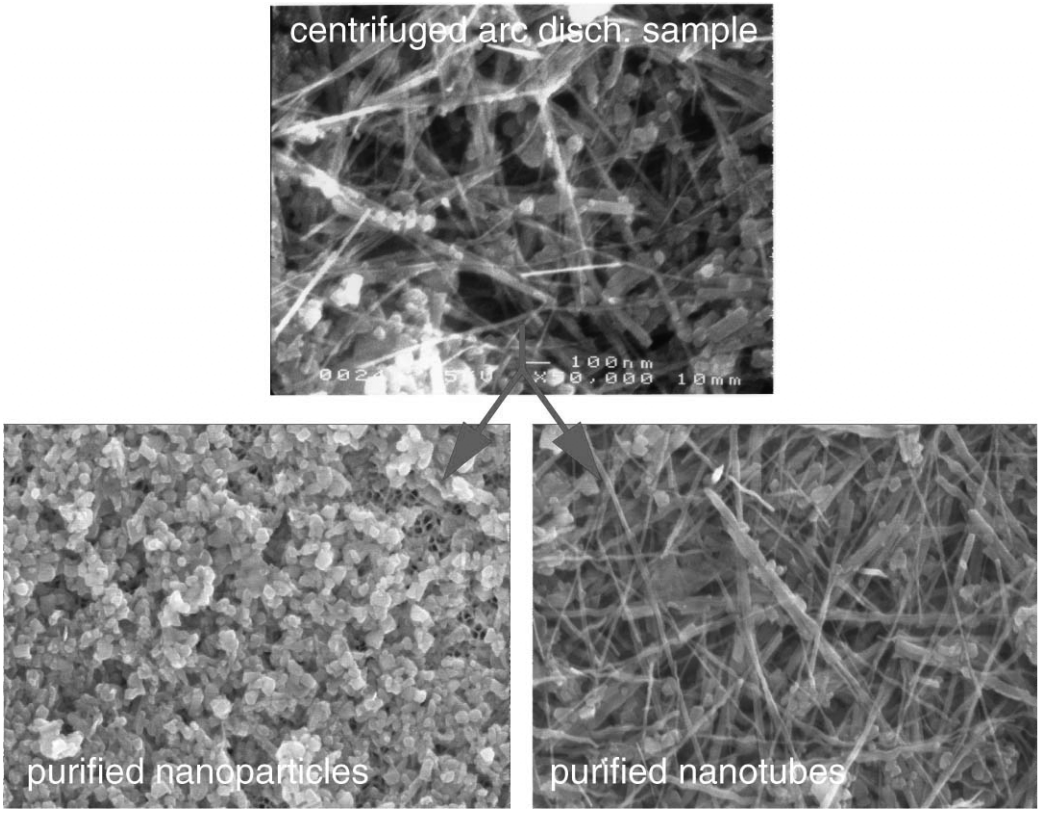

Figure 1. Scanning electron (SEM) micrographs of a MWNT deposit (top) and MWNTs after purification and as a "side-product ", nanoparticles of carbon.

For SWNTs, the purification of the raw soot has been carried out by oxidative dissolution of the carbon encapsulated metal particles with concentrated acid, which ensures maximum efficacy of the process of metal elimination. A weighed amount of the raw soot was sonicated in an ultrasonic bath at 25 ˚C with concentrated nitric acid for a few minutes and subsequently refluxed for 4-6 h. Thick brown fumes containing oxides of nitrogen were seen, indicating the rapid oxidation of carbon to carbon dioxide. After cooling, water was added so as to leave the samples in 6M HNO_3 for the next 8-12h, after which, it was centrifuged several times and the supernatant rejected until the pH of the solution was around 6.5. High resolution transmission electron microscopy of the material from this solution

showed the presence of long ropes of bundled nanotubes accompanied by small amounts of carbon-coated metal particles. Parallel examination of the unpurified soot indicated that more than 80% of the metal had been dissolved. The SWNTs in suspension were stabilized by using a surfactant such as SDS and left undisturbed for 3-5 days until the slow aggregation of the nanotubes allowed their separation from the nanoparticles in solution. The nanotube suspension was filtered through a polycarbonate membrane (1 μm pore size) in order to eliminate most of the particles. On drying, the sediment on the filter paper peeled away to form a self supporting sheet of carbon nanotubes. Scanning electron micrographs of such a sediment, like the one in Fig. 2 shows a network of SWNTs.

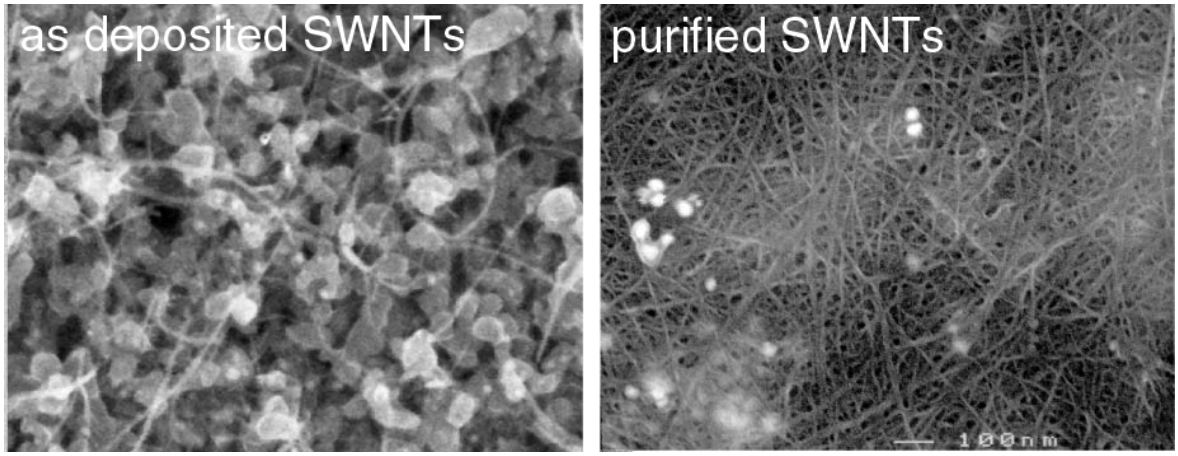

Figure 2. Scanning electron (SEM) micrographs of (a) a SWNT deposit and (b) a mat of SWNTs after purification. A few nanoparticles and embedded catalyst particles are still present.

MWNTs are also prepared by catalytic decomposition of acetylene (or other carbon-containing materials) over supported transition metal catalysts in a temperature range of 700-800^{o}C. This reaction can be carried out under relatively mild conditions in a fixed bed flow reactor at atmospheric pressure. After optimization, the catalytic method can be suitable for the production of either single and multiwall or spiral carbon nanotubes.

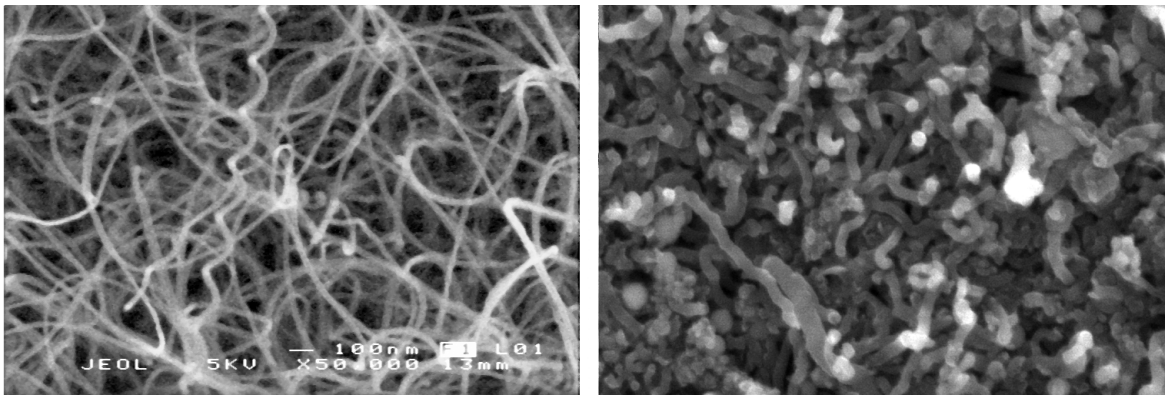

Figure 3. Scanning electron (SEM) micrographs of MWNTs prepared by catalytic decomposition of acetylene.

A further advantage of this method is that it enables the deposition of carbon nanotubes on pre-designed lithographic structures[2], producing ordered arrays which can be used in applications such as thin-screen technology, electron guns etc. The feasibility of the deposition of carbon nanotubes on a ceramic membrane and its field emission properties was demonstrated.

MECHANICAL PROPERTIES

It is becoming clear from recent experiments[3-9] that carbon nanotubes (CNTs) are fulfilling their promise to be the ultimate high strength fibres for use in materials applications. There are many outstanding problems to be overcome before composite materials, which reflect the exceptional mechanical properties of the individual nanotubes, can be fabricated. Arc-discharge methods are unlikely to produce sufficient quantities of nanotubes for such applications. Therefore, catalytically grown tubes are preferred, but these generally contain more disorder in the graphene walls and consequently they have lower moduli than the arc-grown ones. Catalytic nanotubes, however, have the advantage that the amount of disorder (and therefore their material properties) can be controlled through the catalysis conditions, as mentioned before. As well as optimizing the material properties of the individual tubes for any given application, the tubes must be bonded to a surrounding matrix in an efficient way to enable load transfer from the matrix to the tubes. In addition, efficient load bearing within the tubes themselves needs to be accomplished, since, for multi-walled nanotubes (MWNTs), experiments have indicated that only the outer graphitic shell can support stress when the tubes are dispersed in an epoxy matrix[10], and for single wall nanotube (SWNT) bundles (also known as ropes), it has been demonstrated that shearing effects due to the weak intertube cohesion gives significantly reduced moduli compared to individual SWNTs[6]. The reduced bending modulus of these SWNT bundles is a function of their diameter. An individual tube has an elastic modulus of about 1 TPa, but this falls to around 100 GPa for bundles 15 to 20 nm in diameter. In summary, there are two main challenges to address: to enable strong bonding between the CNTs and the surrounding matrix; to create crosslinks between the shells of MWNTs and also between the individual SWNTs in SWNT bundles, so that loads can be homogeneously distributed throughout the CNTs. Ideally, both these goals should be achieved without compromising the mechanical properties of the CNTs too drastically. Efforts within this group have begun to address these problems using post production modification of CNTs via chemical means and controlled irradiation.

High resolution transmission electron microscopy (HRTEM) can be used to give invaluable information about the structure of CNTs, in particular, the amount of order/disorder within the walls of MWNTs. Atomic force microscopy (AFM) can be used to measure the mechanical properties of individual CNTs[4-7]. Use of both techniques has allowed us to make a correlation between the strength of MWNTs, grown in different ways, with the amount of disorder within the graphene walls (see below).

The AFM technique developed in our laboratories has already enabled characterisation of the moduli of SWNT bundles[6] and MWNTs, both arc-grown and catalytically grown[7]. The method has been described in detail previously[6,7]. Briefly, it involves depositing CNTs from a suspension in liquid onto well-polished alumina ultrafiltration membranes with a pore size of about 200 nm (Whatman anodisc). By chance, CNTs occasionally span the pores and these can be subjected to mechanical testing on the nanometer length scale. Contact mode AFM (M5 Park Scientific Instruments) under ambient conditions is used to collect images of the suspended CNTs at various loading forces. Fig. 4 shows an AFM image of a SWNT bundle suspended across a pore and a schematic representation of the mechanical test. The maximum deflection of the CNT into the pore as a function of the loading force can be used to ascertain whether the behavior is elastic. If the expected linear behavior is observed, the Young's modulus can be extracted using a continuum mechanics model for a clamped beam configuration[6,7]. The suspended length of the CNT, its deflection as a function of load and its diameter can all be determined from the images, enabling the modulus to be deduced. The diameter is taken as the height of the tube above the membrane surface at the clamped ends. Although tip convolution can be a problem in measuring lateral dimensions using AFM, the height is a reliable measure because the CNTs are essentially incompressible at these loads (nominal loading forces are in the range 1 to 5 nN). The suspended length can be determined from line profiles taken either side of the tube. A minimum suspended length is measured

because of the convolution of the tip with the edge of the pore. This means that all the determined moduli quoted here are minimum values.

The powerful advantage of the AFM technique employed in our laboratory is its simplicity. There is no need for complex lithographic techniques for suspending and clamping tubes. The surface forces between the CNTs and the alumina membrane are sufficiently high to maintain the clamped beam condition in the majority of cases. In addition, the nanotubes are never exposed to electron radiation during measurement, which is the case for TEM studies. Radiation will induce defects, if the energy of the electrons is high enough, and thereby alter the material properties. This is one effect that we are currently utilising in a positive way in an effort to modulate CNTs' mechanical properties. The relative ease of sample preparation in our AFM method enables a high measurement throughput allowing us to measure a variety of CNTs synthesized in different ways and to compare the results. Described below are new data on catalytic MWNTs, and arc-grown SWNT bundles that have been hydrogenated and exposed to a low-level of radiation. Catalytic MWNTs were produced through decomposition of acetylene over a cobalt/silica catalyst. The previously measured catalytic MWNTs were produced at a temperature of 900^{o}C [11], whereas the new data presented here were obtained on MWNTs fabricated at 720^{o}C. The microstructure of the catalytic MWNTs has a strong dependence on the synthesis temperature which can be readily seen via HRTEM.

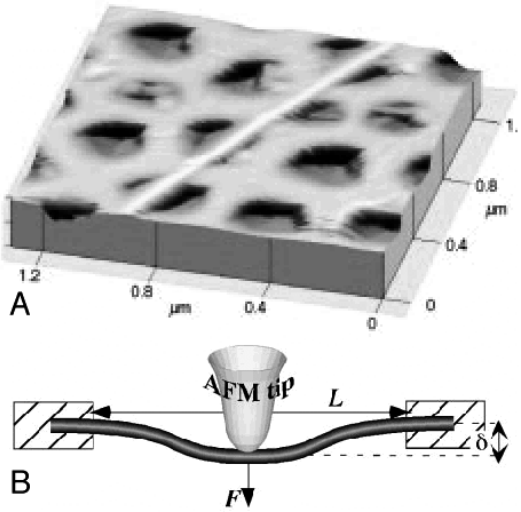

Figure 4. (a) 3D rendering of an AFM image of a SWNT bundle adhered to the alumina ultrafiltration membrane, leading to a clamped beam configuration for mechanical testing. (b) Schematic representation of the measurement technique. The AFM applies a load, *F*, to the portion of nanotube with a suspended length of *L* and the maximum deflection *d* at the center of the beam is directly measured from the topographic image, along with *L* and the diameter of the tube (measured as the height of the tube above the membrane).

To produce crosslinks between the shells of MWNTs and between the SWNTs of SWNT bundles, the sp^2 carbon bonding must be disrupted to sp^3 bonding so that dangling bonds are available for crosslinking. Since the sp^2 bonding is the essence of the CNTs strength, this must not be disrupted to such a degree that the properties of the individual shells in MWNTs or individual SWNTs in bundles are degraded. Hydrogenating CNTs is a first step towards producing them with internal crosslinking. The MWNTs and SWNT bundles were hydrogenated using a modified Birch reduction using Lithium and methanol in liquid ammonia[12]. The SWNT bundles were subsequently exposed to 2.5 MeV electrons with a total radiation dose of 11 C/cm^2. A theoretical estimation of the number of displacements that this dose produces suggests that it will create about 1 defect per 360 carbon atoms[13].

AFM measurements on the hydrogenated, irradiated SWNT bundles are shown in Fig. 5, along with the previous measurements of untreated SWNT bundles[6]. As before, the bundles were dispersed in ethanol using an ultrasonic probe and deposited on the alumina membranes for measurement by AFM in air. Within the errors of our measurement technique a

strengthening of the bundles was not observed: the Young's modulus still decreases in a similar trend to the as-grown bundles. However, the treatment does not appear to have compromised the strength of the individual SWNTs either, since the lower diameter bundles have comparable moduli. In addition, it was noticed that the treated bundles were more difficult to disperse in ethanol and the morphology of the sample in the AFM showed that the bundles exhibited a higher degree of aggregation. Taken together these data suggest that the radiation treatment produced bonding between the tubes but was not sufficient to produce enough crosslinks within the bundles to reduce shearing effects and produce bundles with higher Young's moduli. Future efforts will concentrate on optimising the chemistry and irradiation doses to improve their mechanical properties.

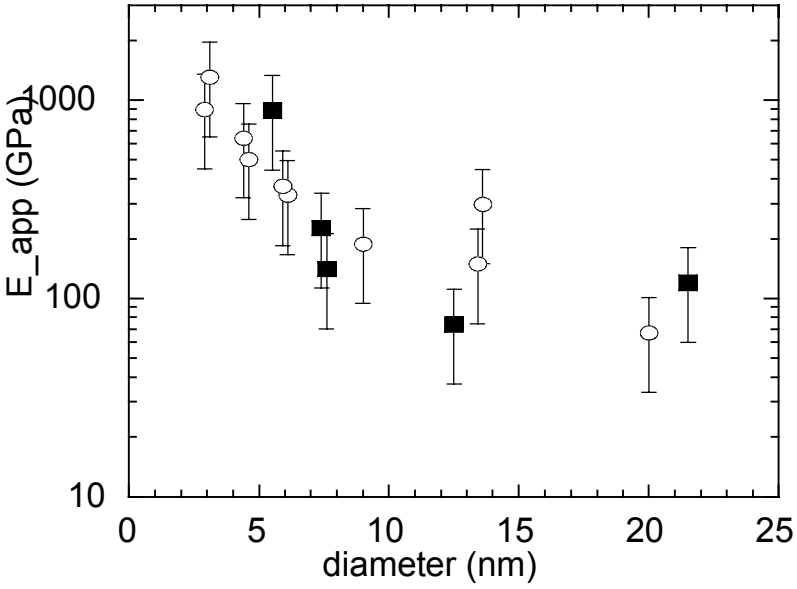

Figure 5. Dependence of the apparent Young's modulus (E_app) on the diameter of SWNT bundles meaured using AFM. The untreated bundles are represented by the open circles and the hydrogenated and irradiated bundles by the filled squares.

Previous AFM measurements of the mechanical properties of MWNTs, arc-grown and catalytically grown, are compared with catalytic MWNTs grown at different temperatures. These data are summarised in Fig. 6, along with HRTEM data showing qualitatively the amount of order/disorder within the walls. As one might expect, the Young's modulus of the MWNTs decreases as the disorder within the walls increases. Arc-grown MWNTs, which contain very few defects, have a modulus comparable with that measured for an individual SWNT[6,7]. The moduli of catalytic MWNTs can vary depending on the structure. Those measured previously[7] were very disordered and had a kind of stacked coffee cup structure (see Fig. 6b, part iii). The other catalytic MWNTs, grown at a lower temperature, showed a higher degree of order within the tubes and consequently had slighty higher moduli. The dispersion of the measured values in this case was large. This could be due to greater uncertainties in the measurement technique, since these MWNTs were usually curved, making the continuum beam approximation less valid. Previous structural characterisation by TEM has shown that they can have a helical morphology, like the cord on a telephone[14]. However, HRTEM images also indicate that the defect morphology varies along the tubes. This would explain why the measured Young's modulus can vary considerably (remembering that our technique measures the modulus over a section of the CNT 200 nm long).

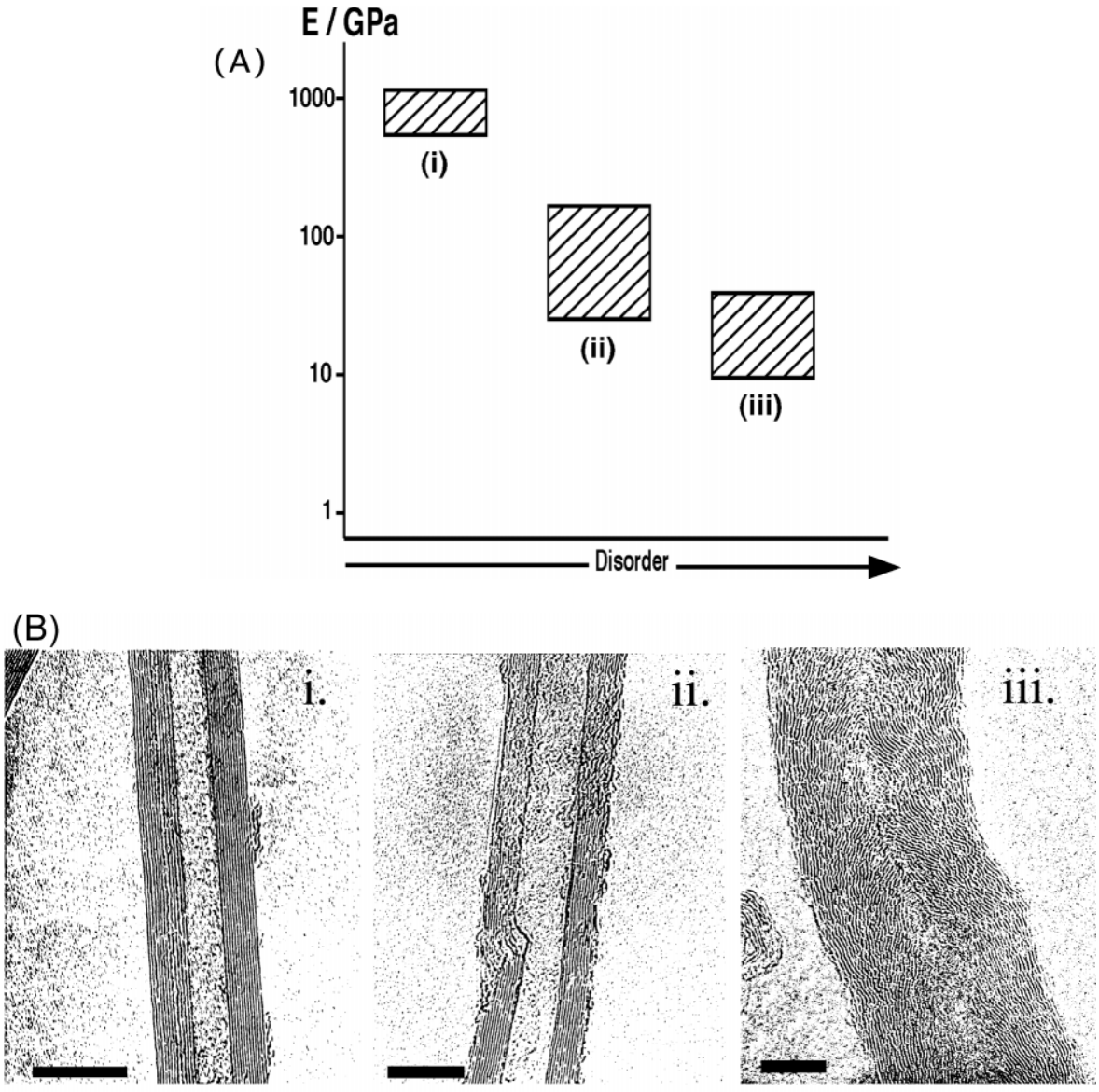

Figure 6. Correlation of the measured Young's modulus of MWNTs with the amount of disorder present with the graphitic walls. (A) Ranges of measured moduli for three different types of MWNT against an arbitrary scale of increasing disorder. (B) The amount of disorder seen in HRTEM data can be qualitatively ranked to make the correlation. MWNTs were produced via, i) arc-discharge, and decomposition of acetylene using a Co / silica catalyst, ii) at 720^{o}C and iii) at 900^{o}C. All scale bars are 10 nm.

There is some contention about whether the elastic modulus of MWNTs varies as a function of their diameter. Poncharal et al.[8] have recently suggested a rippling mode on the surface of bent MWNTs with diameters greater than about 15 nm, leading to a reduction in the measured modulus. However, a strong dependence of the measured modulus on the diameter was not observed in our previous AFM measurements[7]. It is conceivable that the measurement of the modulus is force dependent and the transition to the rippling mode is not reached with the loading forces used in the AFM experiments. TEM data show rippling on the compressed side of statically bent MWNTs, but these have rather high curvatures[8,15] (much higher than the AFM experiments). Interestingly, we have observed rippling on the compressed sides of the catalytic MWNTs. Fig. 7 shows a high resolution AFM image of a catalytic MWNT (grown at 720^{o}C) lying across a pore, the edge of which can be seen on the left of the image. It clearly shows rippling only on the right-hand side of the tube, the direction in which the CNT is bent, which has a period of roughly 16 nm. These ripples are not perpendicular to the tube axis but are inclined at approximately 30^{o}, making the CNT left-

handed. This rippling could be an inherent structure of the catalytic MWNTs or it could arise from the surface forces, which constrain the CNTs on the membrane. However, rippling can also arise when the tubes are loaded in the AFM. Rippling on the upper, compressed side of these MWNTs has also been observed as the imaging force is increased. Non-linear behaviour in the loading/unloading characteristics of the catalytic tubes was frequently noticed. This also contributes to the uncertainties in measuring moduli on these kinds of MWNTs. It is conceivable that the onset of rippling will occur at lower curvatures, i.e. lower forces, in tubes with a higher amount of disorder.

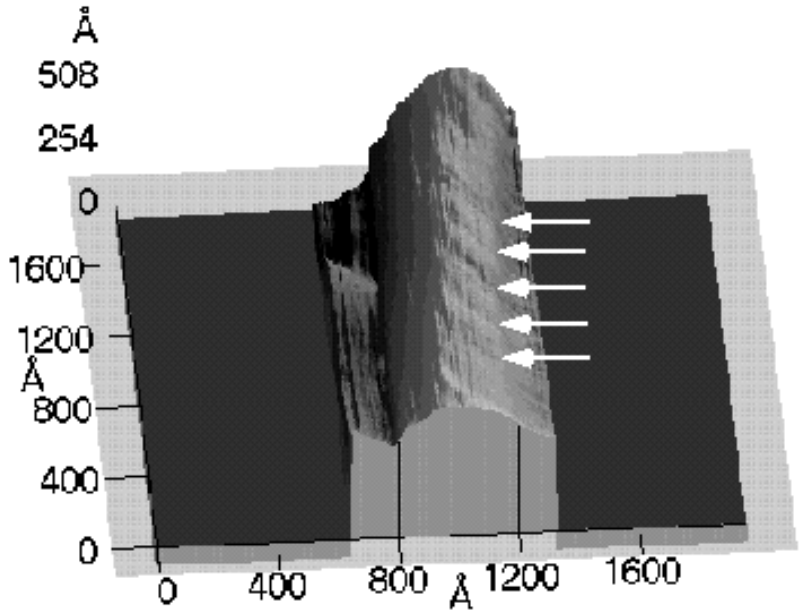

Figure 7. 3D rendering of a high resolution AFM image of a catalytic MWNT, grown at 720^{O}C, suspended on the alumina ultrafiltration membrane. Rippling is observed on the innner side of the natural curvature of the CNT, with a periodicity of about 16 nm, inclined at 30^{O} to the tube axis.

To conclude this section on the measurement of mechanical properties, we have demonstrated that the Young's modulus of MWNTs correlates to the amount of disorder in the graphene walls. Initial attempts at modulating their structure and consequently their mechanical properties have not produced the desired effect, but we believe that chemical modification of CNTs and radiation treatment will be the way forward for improving and/or customising the properties of CNTs for use in composite materials. The radiation doses used to date on the SWNT bundles also did not eliminate the shear behaviour of the SWNTs within the bundles, but observed differences in their propensity to dispersion and greater aggregation of the bundles observed in the AFM, indicates that the surface chemistry of the bundles has been modified, which gives hope that these methods will soon become fruitful. We expect that there will be an optimal radiation dosage, which introduces enough crosslinks between the SWNTs, to improve the moduli of the bundles, but is not sufficient to introduce enough disorder to seriously reduce the modulus of an individual SWNT.

TRANSPORT PROPERTIES

Carbon nanotubes are molecular wires whose electronic properties are largely determined by extended molecular orbitals. Depending on the specific realization, the

nanotube may be a true one-dimensional metal or a semiconductor with a gap. By combining metallic and semiconducting tubes the whole span of electronic components ranging from wires, bipolar devices to field-effect transistors[16] may be embodied in nanotubes.
On the fundamental side, a perfect metallic nanotube is supposed to be a ballistic conductor in which only two one-dimensional (1d) subband carry the electric current[17]. Hence, the conductance should be given by $G = 4e^2/h = 6.4\ k\Omega^{-1}$ independent of the NT diameter d.

Carbon nanotubes, especially SWNT are considered as prototypes of 1d conductors. The electronic properties of one-dimensional conductors have generated a lot of interest both experimentally and theoretically. The reason for this excitement lies in the very rich phase diagram of a 1d conductor (expressed in "g-ology") and the prediction that in a 1d system Coulomb interactions should lead to a strongly correlated electron gas, called a Luttinger liquid (LL), instead of the usual quasi-particle picture described by a Fermi-liquid. Experimentally, the systems that were the closest to these expectations were the organic linear chain compounds like TTF-TCNQ, $Qn(TCNQ)_2$, TMTSF and TMTTF salts[18]. There are a lot of interesting transport studies on individual SWNTs, or on ropes of SWNTs (see the contributions of C. Dekker and P. Avouris in this volume). However, there are still unresolved questions concerning their purity (due to their synthesis with magnetic catalysers), the interaction with the substrate, the role of unintentional doping during the purification etc. We have addressed the effect of doping of SWNTs and in order to separate intrinsic and contact effects, we have studied both d.c. and optical conductivities.

Because MWNTs consists of several concentrically arranged SWNTs, one would expect that MWNTs do not qualify as 1d conductors. If adjacent carbon shells interact as in graphite, electrons may not be confined to one shell only, so that much more than just 2 subbands (as for a perfect SWNT) could carry the current. However, we have found very strong evidence that the current in MWNTs, contacted by metallic electrodes from the "outside", is to a large extend confined to the outermost SWNT. MWNTs have certain specific advantages: their larger diameter favours low-ohmic contacts, they do not contain magnetic impurities, they have very well ordered structure, high conductivity and their mesoscopic size enables the observation of quantum interference effects like the Aharonov-Bohm effect. The latter magnetotransport measurements can all very well be understood in the traditional Fermi liquid framework and assuming 2d-diffusive transport. However, recent measurements of the tunneling DOS have revealed anomalies quite similar to the features observed in SWNTs which were assigned to LL behavior[19]. Because LL-like 1d-features seem to coexists with Fermi-liquid 2d-features, more work is needed to pinpoint the origin of these anomalies.

Optical conductivity and d.c. transport of single walled nanotubes

It seems that with the synthesis of single wall carbon nanotubes one can study a real 1D system. Depending on the choice of the chiral vector, which defines the orientation of the unit cell to the tube axis, the nanotube is either a metal, a narrow gap semiconductor or an insulator. Although the chirality cannot be controlled during the synthesis, STM studies show that 30-40 % of the SWNTs are metallic. The LL behaviour is expected from these metallic SWNTs [19]. In single SWNT measurements, however, the manifestation of the metallic state is not straightforward since twists of the nanotube or interactions with the surface can strongly perturb the electronic structure. It is believed that in mats of SWNTs (called bucky paper) the metallic nature of the nanotubes manifests itself much more readily, due to the absence of the substrate, despite the mixing in of the intertube contact resistances. Moreover, the carrier density in SWNTs can be changed by doping, as in the case of graphite[20]. In order to have a clear picture of the effect on the transport properties of the charge transfer upon doping, it is necessary to understand the interplay between different sources of transport: namely, the transport primarily induced by on-tube doping or governed by the doping of the intertube contacts. In this respect, we have performed dc transport measurements and optical experiments on pristine and potassium doped bucky paper samples.

Fig. 8a shows the d.c. transport of the pristine SWNT and the K-doped sample. Fig. 8b. displays the optical conductivity for the same samples. The pristine sample shows a Drude component in the optical conductivity despite the non-metallic behaviour in dc resistivity

measurements. We attribute this disagreement to effects relating to the non-metallic intertube contacts, which will affect the d.c. transport. Potassium doping renders the nanotubes more metallic, the d.c. resistivity slope is positive in a wide temperature range. This is partly due to improved nanotube rope-rope contacts and to the increased carrier density of the tubes. It also turns out that the potassium doping influences the tube-tube contact regions much more strongly than the intrinsic on-tube transport, so that the average dc-conductivity is higher than the ω=0 optical contribution, averaged over all directions.

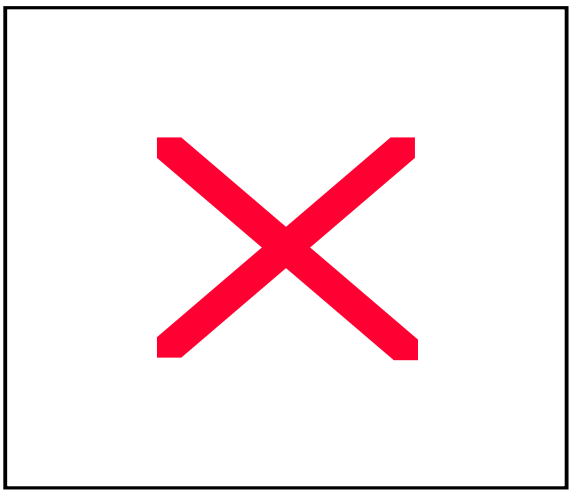

Figure 8a. d.c. resistivity of pristine and potassium doped SWNT thick film. The stoichiometry of the K-doped samples is close to KC_{16}.

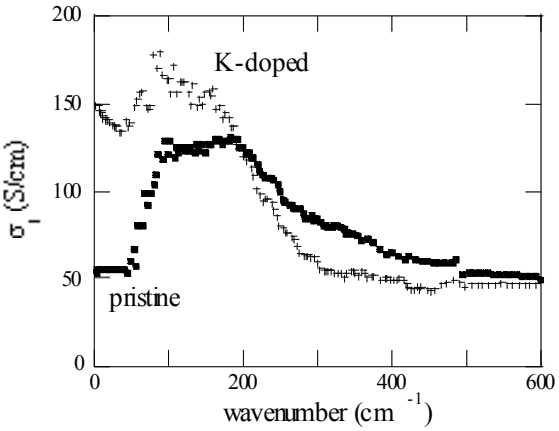

Figure 8b. Optical conductivity of pristine and potassium doped SWNT thick film. The stoichiometry of the K-doped samples is close to KC_{16}.

Transport of multiwalled nanotubes

Electric transport measurements for single multiwall nanotubes (MWNTs) contacted by four metallic Au fingers from above will be discussed. An example of a device is shown in Fig. 9. Observed interference corrections to the resistance allow to determine the degree of scattering (elastic-scattering length l_e and phase-coherence length l_ϕ). Tunneling spectroscopy, on the other hand, is used to determine how strongly the single-particle density-of states (DOS) is modified by interactions (e.g. Coulomb interaction). Low-ohmic contacts < 10 kΩ are used for measuring the equilibrium (two- or four-terminal) conductance[21] and a high-ohmic contact > 100 kΩ is employed in a tunneling spectroscopy experiment in which the differential conductance dI/dV is measured as a function of V and temperature[22].

Four-terminal electrical resistances R_{4t} have been measured as a function of temperature, T, in a He-3 system down to T≈0.3 K. The resistance always increases with decreasing temperature and appears to saturate around 1-4 K. A typical example is shown in Fig. 10. Note that this saturation has recently been identified to be of extrinsic origin. It is caused by electron heating induced by rf-radiation in the measuring leads. The increase of R from room temperature down to Helium temperatures is moderate amounting to a factor of ≤ 2-3. This is taken as evidence for the metallic nature of the MWNTs.

We emphasize that not only is the temperature dependence of R(T) similar for all samples, but the absolute resistance values also fall into a relatively narrow range of R_{4t}≈2-20 kΩ. The increase of resistance at low temperatures is markedly different from (HOPG)

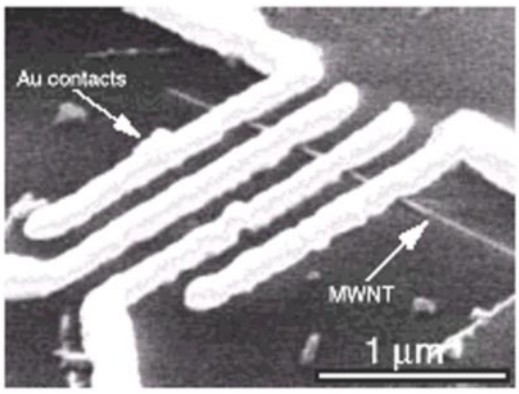

Figure 9. Scanning-electron microscopy image of a single multiwall nanotube (MWNT) electrically contacted by four Au fingers from above. The separation between the contacts is 350 nm center-to-center.

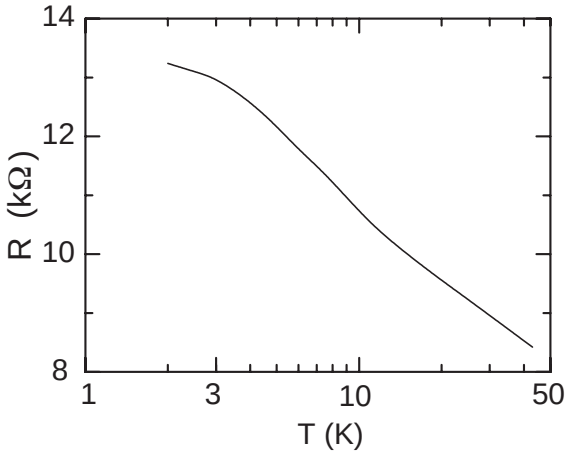

Figure 10. Typical temperature dependent electrical resistance R(T) of a single MWNT measured in a four-probe configuration, i.e. the current is passed through the outer contacts and voltage is measured over the inner ones.

graphite. For HOPG the resistivity decreases with decreasing temperature as commonly associated with metallic behavior. In trying to understand the temperature dependence of R, we first consider the simplest possible model. We will compare the absolute measured resistance values with an expression for the classical Drude resistance taking one graphene cylinder and assuming 2d-diffusive transport, i.e. assuming $l_e << \pi d$. We thereby completely disregard the quantization of the wavevector around the tube circumference leading to 1d subbands. The electron states have energy $E = \pm (h/2\pi)\, v_F|\mathbf{k}|$, where $\mathbf{k}$ is the 2d-wavevector measured with respect to the two independent Brillouin corner points. The Fermi energy is taken to be $E_F=0$ and a reasonable value for the Fermi velocity $v_F=10^6$ m/s is assumed. For the electron density-of-states (DOS) we obtain $n_{2d}(E) = 2E/\pi(hv_F/2\pi)^2$. Using the Einstein equation $\sigma_{2d} = e^2\, n_{2d} D$, which relates the conductivity σ_{2d} to the diffusion coefficient $D=v_F\, l_e/2$ and the electron density, the energy-dependent conductivity is found to be $\propto E$. To obtain the equilibrium sheet conductivity σ_{2d} at finite temperature, the energy has to be replaced by kT, leading to:

$$\sigma_{2d} \approx \left(\frac{2e^2}{h}\right)\frac{kT}{hv_F} l_e$$

Due to the vanishing electron DOS for $E \rightarrow 0$, the resistance of a graphene sheet increases with decreasing temperature following $R(T) \propto T^{-1}$. Although a resistance increase is observed, the increase is not compatible with a T^{-1} dependence. Moreover, putting in numbers results in a unreasonably large mean-free path l_e. Taking from the experiments, R=10kΩ, contact separation L = 350 nm, tube diameter d = 20 nm and T = 4 K, we obtain $l_e \approx 13$ µm. This large mean-free path violates the assumption that diffusion is 2-dimensional. Even more serious, $l_e >> L$. The only way to reconcile this model with the requirement that $l_e \leq L$ is to assume that a large number (30) of graphene cylinders carry the electric current equally. We know from the Aharonov-Bohm experiments that this is not the case (see below)[23]. We therefore conclude that the specific temperature dependence of R cannot be related to the energy-dependent DOS of graphene. Within this simple Drude picture, the discrepancy can, however, be resolved if we take into account the band-structure modifications imposed by the periodic-boundary condition along the circumference of the cylinder leading to 1d-subbands. In contrast to graphene, for which the DOS tends to zero as $E \rightarrow 0$, the DOS is constant in a relatively large energy window centered around the Fermi energy. This energy window is given by the subband separation ΔE_{sb} which should be inserted instead of kT into the previous equation. With ΔE_{sb}=100 meV, typically valid for the outermost cylinders of our MWNTs, one arrives at a mean-free path of $l_e \approx 50$ nm, which is of order of the circumference of the tube. This number is of reasonable magnitude and in agreement with magnetoresistance

measurements. This argument suggests that electron transport in MWNTs is not purely 2d-diffusive. More importantly, it demonstrates that the 1d-subbands need to be considered in MWNTs as well.

The classical 1d-Drude resistance due to static-disorder alone predicts a temperature-independent resistance. Temperature dependences can be caused by other scattering mechanisms, like electron-phonon, electron-electron interactions, and quantum interference corrections. Magnetoresistance (MR) measurements indeed show that the intereference and interaction contributions to the resistance are large and display the required temperature-dependence. Particularly attractive for the investigation of interference phenomena in carbon nanotubes is the fact that they are composed of cylindrical graphene sheets. Nanotubes are therefore *hollow* conductors on the molecular scale with diameters ranging from 1 to 20 nm. In such a geometry, with the magnetic field along the nanotube axis, nanotubes provide a unique model system for the investigation of quantum interference in conducting macromolecules by virtue of the Aharonov-Bohm (AB) effect. Fig. 11 displays such magnetoresistance measurements in a parallel field, which show pronounced oscillations (AB effect)[23]. The oscillations are associated with the weak localization, a quantum-mechanical treatment of backscattering of electrons, which contains interference terms adding up constructively in zero field. Backscattering is thereby enhanced, leading to a resistance larger than the classical Drude resistance. In the usual geometry for films/wires, in which the magnetic field is applied perpendicular to the film/wire, these interference terms cancel in a magnetic field of sufficient strength. In contrast, for a hollow conductor in a parallel field, the magnetoresistance is periodic in the magnetic flux penetrating the hollow tube, with period h/2e. This periodic contribution is due to closed counterpropagating electron trajectories that encircle the tube circumference. This result has given compelling evidence that l_φ can exceed the circumference of the tube so that large coherence lengths are possible for MWNTs. The AB-MR agrees with theory *only*, if the current is assumed to flow through one or at most two metallic cylinders with a diameter corresponding to the measured outer diameter of the NT. We note, that it is not possible to relate the peak separation to h/e because a nanotube diameter would result which is larger than the actually measured diameter. In contrast, taking an AB flux of h/2e results in a diameter compatible with the measured one. Because the h/2e period requires backscattering on the scale of the diameter of the NT it is clear that the NTs are *not ballistic*.

In addition to the resistance oscillation, which agrees with the magnetic-field period as derived from the cross-section, unexpected short-period oscillations have also been discovered[23]. It was suggested that the short period oscillations are due to chiral currents in strained nanotubes. Chirality is a well estabilished structural property of carbon nanotubes. In principle, graphitic tubules have isotropic conductivity, however, when they are mechanically stretched due to the interaction with the substrate, or due to thermal contraction, the honeycomb lattice can be distorted resulting in an anisotropic, chiral current. Chirality can select special winding numbers which give the higher order term superimposed on the long period oscillations. In a MWNT the chirality can change from layer to layer, and the period of short oscillations can vary from tube to tube and from sample to sample. This fine structure in the AB oscillations is a completely new phenomenon, which we believe is closely related to the special structure of the carbon nanotubes.

From the width of the zero-field resistance peak of Fig. 11 the phase-coherence length l_φ is estimated to be $l_\varphi \approx 200$ nm. As a test for consistency the WL correction to the conductance ΔG is compared with the measurement. Taking L=350 nm and $l_\varphi = 200$ nm we obtain $\Delta G = 4.4\ 10^5$ S, which is in very good agreement with the measured conductance change of $\Delta G = 4.6\ 10^5$ S. From MR measurements in a perpendicular field similar coherence lengths are deduced. Because $l_\varphi(T)$ has a temperature-dependence which agrees with the expected Nyquist-type dephasing, the comparison with theory allows the elastic-scattering length l_e, to be deduced. We obtain l_e =90-180 nm[22]. Because $l_e \geq \pi d$, transport in our MWNTs should be classified as *quasi-ballistic*.

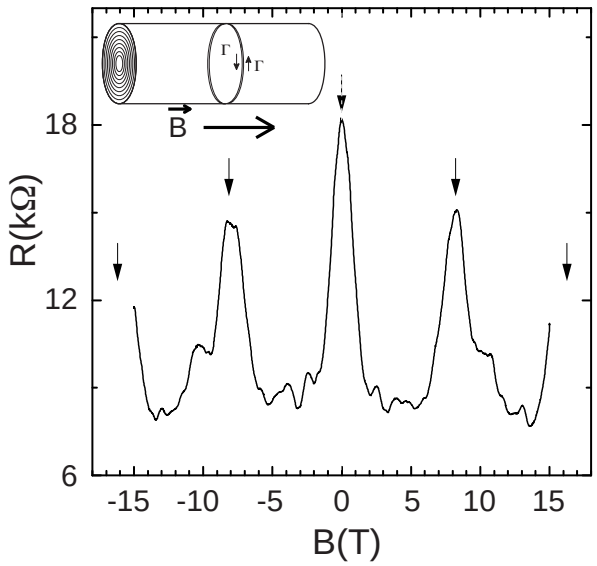

Figure 11. Electrical resistance R as a function of magnetic field B of a MWNT aligned parallel to B. Arrows denote the resistance maxima corresponding to multiples of h/2ein magnetic flux through the nanotube taking the *outer* diameter

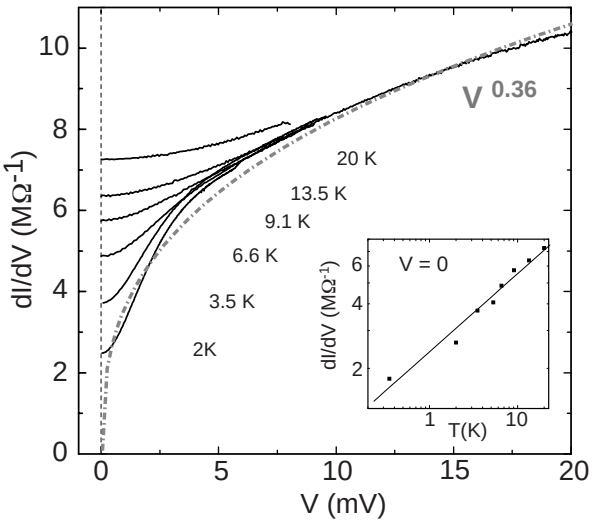

Figure 12. Differential tunneling conductance dI/dV measured on a single MWNT at different temperatures T displaying a pronounced zero-bias anomaly. Inset: log-log representation of dI/dV vs. T for V=0. The dashed-dotted curve displays the power law $dI/dV \propto V^{\alpha}$ with $\alpha = 0.36$ deduced from the inset.

There are two other independent observations in favor of this result. 1) van Hove type singularities have been seen in a dI/dV tunneling spectrum[22]. Because these features are associated with the formation of 1d-subbands, l_e should be of order of, or larger than, the circumference of the NT. 2) as shown before, the measured resistance values ≈10 kΩ can only be explained if the DOS is considered to be 1d. However, the resistance contains a contribution that grows with length. The length-dependence amounts to ≈ 6 kΩ/μm at room temperature. Using the Landauer formula one obtains an effective transmission coefficient of T=0.5 per micrometer length. Hence, the mean-free path must be large. The observed van-Hove type dI/dV spectra[22] demonstrates that the peculiar bandstructure effects of SWNTs are also found for MWNTs. We have to emphasize, however, that a spectrum with sharp van-Hove singularities, in close agreement with tight-binding calculations, has only been observed on one sample until now. The prevailing spectra display a pronounced zero-bias anomaly (ZBA) on a smaller energy scale of 1-10 meV. For larger energies, a peak-structure develops in dI/dV on the scale of the subband separation, 0.1eV, which may be associated with (broadened) van-Hove singularities.

A typical ZBA is shown in Fig. 12 for six temperatures ranging from 2-20 K. A suppression of the tunneling DOS is expected for a strongly correlated electron gas [24]. Similar anomalies have recently been observed by Bockrath *et al.* for SWNTs[19]. Their measurement and analysis provide the first demonstration for possible Luttinger liquid (LL) behavior in carbon NTs due to long-range Coulomb interactions. LL theory predicts power laws both for the voltage and temperature dependence with the same exponent α. A power-law with $\alpha \approx 0.36$ is deduced from dI/dV(T,V=0); see the inset of Fig. 12. For comparison with the observed dI/dV-voltage dependence, the dashed-dotted curve $\propto V^{0.36}$ has been plotted. The same exponent $\alpha = 0.36$ was obtained by Bockrath *et al.* This exact agreement has presumably no significance because we use single MWNTs whereas they have used SWNT ropes. On the other hand, the agreement may indicate that the same physics is responsible for the ZBA.

The reported study of electric transport of single MWNTs gives rise to results which appear to be in contradiction. For example, the observation of an Aharanov-Bohm effect with period h/2e suggests diffusive transport on the scale of the circumference of the nanotube, i.e. $l_e \leq \pi d$. On the other hand, we have observed a dI/dV spectrum which agrees with tight binding models assuming the existence of 1d-subbands. This suggests the opposite, i.e. $l_e \geq \pi d$. Our results are therefore consistent only if l_e is of the order of the circumference. There is

a second `contradiction': on the one hand, we have used weak-localization theory which is based on the Fermi liquid hypothesis; on the other hand, the observed suppression of the single-particle of states suggests that NTs may develop a Luttinger liquid (LL) state. If an LL is the correct description for NTs (including MWNTs) we need to know how the observed quantum interference corrections have to be described. Is there something similar as weak localization in the LL picture? What happens in a magnetic field?

ELECTRON SPIN RESONANCE

Since the pioneering work of Wagoner on graphite[25], Electron Spin Resonance (ESR) has been used intensively to study the electronic properties of graphitic or conjugated materials. One of the advantages of the method is to give information both on localised spins and conduction carriers. Three different quantities are provided by ESR: the g-factor, which depends on the chemical environment of the spins via spin-orbit coupling (and hyperfine interaction); the linewidth, which is governed by spin relaxation mechanism; the intensity of the signal, which is proportional to the static susceptibility. In graphite, anisotropy of the band structure induces anisotropy in the g-factor and the linewidth. How is the ESR behaviour modified in carbon nanotubes? Changing the dimensionality from 2D to 1D is expected to significantly modify the main ESR characteristics. In particular, the conduction carrier contribution to the susceptibility should be enhanced in 1D. For metallic tubules, the density of states *per unit length* (independent of the diameter) along the axis is a constant given by: $N(E_f)=8/(\sqrt{3}\pi a_0 \gamma_0)$, where a_0 is the lattice constant and $\gamma_0 \approx 2.5$ eV is the overlap energy. The DOS per carbon atoms is thus a decreasing function of the diameter. It is worth measuring graphitic nanostructures with different diameters to check this prediction.

ESR of multiwalled nanotubes

Conduction carriers and defect density. Pauli susceptibility of MWNTs, measured from X-band ESR, is comparable to that of graphite. Taking into account the rather large distribution of diameters and lengths in the samples, one can estimate the susceptibility in the approximation of independent shells, i.e. supposing that the interlayer interactions do not modify $N(E_f)$ of MWNTs, in contrast to graphite. Doing this, supposing that 1/3 of the cylinders are metallic, it is difficult to reach the measured value. Moreover, polyhedral multishelled particles (always present in macroscopic quantities of MWNT) have the same susceptibility as MWNTs within an uncertainty of 20%. We speculate that the interlayer interactions can not be neglected for MWNTs and have an important contribution in $N(E_f)$ in a similar way to graphite, i.e. π/π^* overlap occurs between neighbouring shells.

There are only a few studies of defects in carbon nanotubes. It was suspected that arc-grown MWNTs contain a lot of defects that modify their electronic properties[26]. Among these defects, vacancies and interstitials can generate paramagnetic centres that can be detected by ESR. Pentagon-heptagon pair defects can also be present in the lattice. All these defects, which result from displacement of carbon atoms from their pristine location in the hexagonal lattice, should be produced by irradiation and annealed at high temperature. We carried out energetic electron irradiations[27] and annealing of MWNTs to investigate the influence of defects on the ESR behaviour. We found that arc-grown MWNTs contain a very low density of paramagnetic defects, which manifest themselves as a Curie tail in the susceptibility at low temperature. No particular modifications were observed after annealing at 2800°C, in contrast

to ref. 26. The density of paramagnetic defects increases linearly with the electron irradiation dose. We also found that the defects density *per gram* in MWNTs is lower than in polyhedral multishelled nanoparticles, which suggests that imperfections are present in the MWNT tips (Fig. 13).

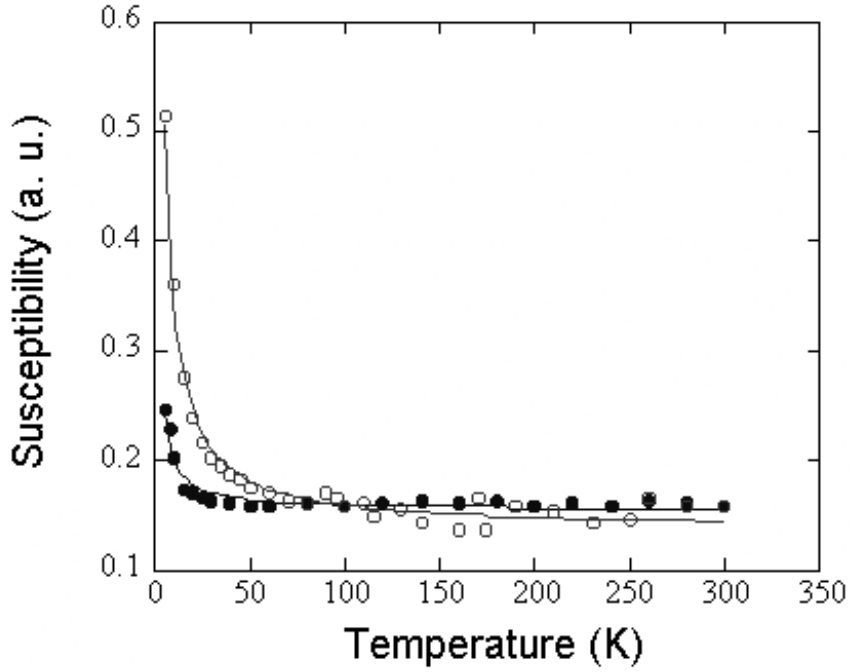

Figure 13. Spin susceptibility vs temperature for MWNTs (filled circles) and nanoparticles (open cirlces). Note that the Curie tail at low temperatureres is smaller for MWNTs than nanoparticles.

g-factor, spin relaxation, and contact broadening effect. The conduction electron spin g-factor is determined by spin-orbit splitting of the energy levels in presence of a magnetic field[28]. In the case of degenerate bands (as in graphite at the K point), theory predicts that spin-orbit coupling, which removes the degeneracy, induces a large g-shift which varies inversely with temperature. This is exactly what happens in graphite when the magnetic field is perpendicular to the plane, allowing large orbital currents. This increases the spin-orbit coupling. When the magnetic field is parallel to the planes, orbital currents are suppressed and a small g-shift nearly independent of temperature is observed. When the Fermi level is shifted away from the K point by doping, degeneracy and the g-shift anisotropy disappear. (Despite this understanding of the variation of g-shift a rigorous theory is still missing in graphite due to the complicated band structure near the point of degeneracy.) Using this qualitative theoretical framework, one can speculate about the g-factor of carbon nanotubes. When the magnetic field is parallel to the tube axis, nearly the same value as found in graphite is expected, except at a field for which the cyclotron radius equals that of the nanotubes. Such fields (typically 1T and greater) are higher than those used in X-band spectrometers, but a small increase of the g-factor at the X-band field (0.33 T) is not excluded. When the magnetic field is perpendicular to the tube axis orbital currents can not completely close, as in a plane, and we can expect a smaller g-shift than in graphite. A decrease of this g-shift with the diameter of the tube is then expected. Some of these predictions are indeed realised in MWNTs. First the average g-value is 2.012 compared with 2.018 in graphite and 2.015 in partly graphitised carbon blacks (the difference is small but significant). Second the anisotropy is lower than in graphite.

Spin relaxation in metals and semimetals depends also on the spin-orbit coupling. More precisely it is the modulation of the spin-orbit coupling by lattice vibrations that causes spin relaxation. It can be shown that in the framework of Elliott's theory the spin relaxation time is proportional to the momemtum relaxation time. When it is governed by thermal phonons an increase of the linewidth with increasing temperature is observed. In graphite, the linewidth increases when the temperature decreases. This behaviour is attributed to motional narrowing over the g value distribution. A decrease of the linewidth when temperature increases is also observed in carbon nanotubes, which is probably due to this motional narrowing. An additional feature is a line broadening that appears when the nanotubes are brought into contact with each other. This behaviour is specific to nanotubes (and nanoparticles) and it is contrary to what happens in graphitized carbon blacks. Indeed, with carbon black particles or fine graphite powder, increasing the contact between grains increases the motional averaging of the g-factor anisotropy which decreases the linewidth. We believe that the inverse effect with nanotubes results from their mesoscopic nature. In effect, the intrinsic spin mean free path on a cylindrical graphene shell is much larger than the real nanotube length. The spin mean free path is already large in graphite, and should be even larger in nanotubes due to the reduced dimensionality. Other extrinsic mechanisms participate in the linewidth. Among them the intershell-intertube hopping, and also reflection by the tips. We speculate that intertube hopping is responsible for the broadening of the linewidth when the contact between nanotubes increases.

ESR of singlewall nanotubes

In spite of our efforts, all the SWNT samples we studied are ESR silent, i.e. no line is detected with our conventional X-band spectrometer, except from ferromagnetic particles which are never completely eliminated by the purification treatment. Recent theoretical and experimental works suggest that the electronic properties of SWNTs are best understood in a Luttinger liquid (LL) model. If the ground state of an LL is antiferromagnetic this could explain the absence of the ESR line. Another possibility is the presence in SWNTs of magnetic impurities with strong coupling which shorten the spin relaxation time so much that the line can not be detected. It is worth focusing on the latter assumption since the absence of an ESR signal (from carbon materials) is not only observed on SWNTs but also on catalytic multiwall tubes for which we know that an intrinsic ESR signal exists. Spin relaxation of metals with local magnetic moments is a well-known problem[29]. Such a strong influence of magnetic particles on the spin relaxation means that they could also alter the momentum relaxation that is the transport properties of SWNT.

Concerning the presence of defects, which can also have important consequences on the transport properties of SWNTs, the same remarks stated for MWNTs hold, i.e. if heptagon-pentagons pairs are present, vacancies should be present too, since their formation energies are similar. Then an ESR signal from defects is expected. To check this, we have irradiated a purified mat of SWNTs with 2 MeV electrons and an ESR line indeed grows with increasing dose. We therefore suggest that ropes contain only a few defects even after the purification treatment. This is an important result since thermal treatment at high temperature destroys the single shell structure so that point defects in SWNTs could not be annealed, contrary to MWNTs.

ELECTRON AND LIGHT EMISSION

Although most of the research conducted on nanotubes since their discovery has been of a fundamental nature, a keen interest is shown for their potential applications. One of these is field emission, since nanotubes rank among the best electron field emitters that are now available[30-35]. Our goal here is to compare the field emission properties of the different types of nanotubes, and to understand why nanotubes are such excellent field emitters.

Emitter fabrication

To realize a field emission source with one nanotube only, we mounted single MWNTs on a supporting gold wire (diameter 20 μm) that was electrolytically etched to a 250 nm radius tip. No adhesive was used, and the tubes were held onto the tip by Van der Waals forces. A typical emitter is shown in Fig. 14(a). We produced nanotube films by a simple and fast preparation method. Nanotubes were dispersed in a solvent (typically water with a surfactant or ethanol) and the resulting suspension was drawn through a 0.2 μm pore silica filter. The film remaining on the surface of the filter was then transferred on a teflon-coated metal surface by applying pressure[30]. The emission surfaces ranged from 0.1 to 25 mm^2 and can be easily scaled up. The main advantages of this method are that it can be used for all types of nanotubes, in contrast to catalytic deposition techniques, and that it is non-destructive, which is not the case for alternative film preparation techniques where the tubes are opened. We studied films made with closed or opened arc-discharge MWNTs, as-produced SWNTs, as well as catalytic MWNTs showing ``coffee-cup'' structures. Their morphology is readily comparable to the SEM micrographs of Fig 1-3.

Emission properties

Single nanotube field emitter. Fig. 14(c) displays a typical I-V curve for a single MWNT (in this case an opened MWNT). Most single MWNT emitters, closed as well as opened, are capable of emitting over an incredibly large current range. The maximal current we succeeded in drawing from one nanotube was 0.2 mA, and MWNTs reach routinely and repeatedly 0.1 mA. This represents a tremendous current density for such a small object, and is actually quite close to the theoretical limit where the tube should be destroyed by resistive heating[32]. This experimental limit is comparable to the one observed by other groups that studied the electronic transport properties of MWNTs[36].

No significant difference was observed between closed and opened MWNTs, except for the most important property: the voltage needed for the emission. In Fig. 15, we compare the I-V performances of a closed and opened MWNT. We noted for all measured samples that opened tubes were far less efficient emitters than as-grown tubes. The voltages needed for a given emission current are typically a factor 2 higher for the opened tubes. In effect, open edges like those depicted in Fig. 15 may have smaller radius of curvature than closed ends, and opened tubes would be expected to emit current at lower applied voltages due to the higher field amplification. Quite surprisingly, the emission characteristics of nanotubes are seriously degraded by opening their ends. Regarding long-term stability and lifetime, stable emission was observed for more than 100 h at 2 μA in high vacuum. Typical behaviour of metallic cold field emitters, i.e., a gradual and reversible decrease due to the formation of absorbed layers, was not observed. Termination of the emission happened on most tips as a catastrophic and irreversible failure. Lifetimes of more than 1400 h have been reported for emission in ultra-high vacuum for one single tube emitting at 0.5 μA[35].

Figure 14. (a) Single MWNT mounted on the tip of an etched gold wire. (b) Optical micrograph of the experimental set-up for field emission : the gold wire is fixed on a support, and placed 1 mm above the cylindrical counter-electrode. (c) I-V characteristics for a single opened MWNT.

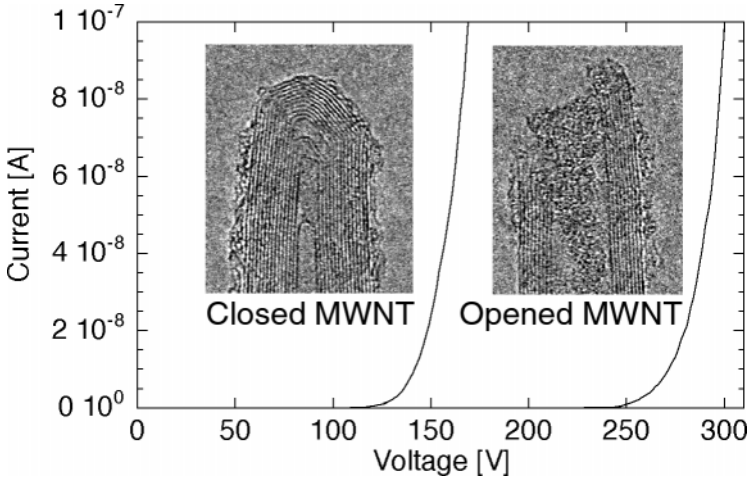

Figure 15. I-V characteristics for a single closed and opened MWNT (the current is given in logarithmic scale), and corresponding TEM micrographs of typical NT tips.

Nanotube film field emitter. We compare in Fig. 16 the field emission performances of four different types of nanotube films. A useful parameter for such a comparison is the electric field (voltage over interelectrode distance V/d) needed to produce a given current density. We found systematically that closed MWNT films displayed lower emission voltages, followed by SWNTs, opened MWNTs and finally catalytic "coffee-cup" MWNTs. To understand the observed differences between the different types of nanotubes, it is instructive to estimate the field amplification factor β from I-V characteristics and corresponding F-N plots[32]. Since this field amplification factor depends only on the geometrical shape of the emitter for a given workfunction and interelectrode distance, we can then directly compare the effective emitter shape of the different nanotube films (by assuming that the workfunction is 5 eV for all tubes). We found that the field amplification factors were significantly higher for singlewall (β =3400) than for multiwall nanotube (β =1600) films. This enhancement is most probably due to the smaller tip radius of SWNTs. The tip radius is also responsible for the low field amplification obtained with the catalytic tubes (β =830) with respect to the closed MWNTs, although the disordered structure of the tip and the high defect density may also have an

influence. However, the difference between closed (β =1600) and opened MWNTs (β =1100) cannot only arise from geometrical considerations, since the variation of mean diameter and length between opened and closed MWNT is rather small, as can be seen in Figure 11 for example. We speculate that most of this difference is due to changes in the work function that arise from the state of the tip. Finally, the above values show that the high density of nanotubes on the film surface may be a disadvantage. For the same experimental conditions, a single MWNT should produce a field amplification of β =6500, and the average value we observe is lower by a factor 4. It appears that the presence of neighboring tubes near the emitters screen the applied field, which results in a lower field amplification.

Figure 16. I-V characteristics for different nanotube films.

In summary, our catalytic tubes showed high emission voltages mainly because of their larger average diameter. The small diameter of SWNT should lead to very low emission voltages, while the SWNT films show "only" comparable performances to closed MWNT films. We suppose that this relative inefficiency arises from the fact that most SWNTs are bundled in ropes, and that these ropes mostly end in catalyst particles. Only few SWNTs tips are detected by TEM, and these protrude only by a few tens of nanometers at most from the sample. This in turn means that the density of free SWNT tips, and thus of potential emission centers, is far lower than for MWNTs. As for the huge difference between closed and opened MWNTs, we noted that our best film emitter with opened tubes didn't even come close in performances to the worst emitter with closed tubes. The observed difference can therefore not be assigned to the quality of the films, and we conclude that it is due in great part to the state of the tip. Interestingly, the only emitters which compete in terms of emission voltage with nanotubes films are diamond-covered Si tips[37]. This indicates that maximal efficiency for film field emitters can be reached only when the emitters are well aligned and placed with their long axis perpendicular to the film substrate, and when the emitters are well separated from one another. We thus infer that carbon nanotube films will have to be realised fulfilling the above-mentioned conditions to reach a maximal emitting efficiency. To our knowledge, the only method to grow aligned and well-separated nanotubes is by catalytic reactions over a patterned substrate, as currently investigated by several groups[34,38,39]. Our results suggest however that care should be taken to obtain well-graphitized, closed MWNTs with small diameters.

Light emission

A rather unusual behaviour linked to the field emission was observed in the form of light emission. This light emission occurred in the visible part of the spectrum, and could sometimes be seen with the naked eye. Typical examples are shown in Fig. 17(a) and (b). This luminescence was induced by the electron field emission since it was not detected without applied potential (and thus emitted current). Furthermore, the emitted light intensity followed closely the variations in emitted current, as can be assessed in Fig. 17(c), where the emitted current and emitted light intensity have been simultaneously measured.

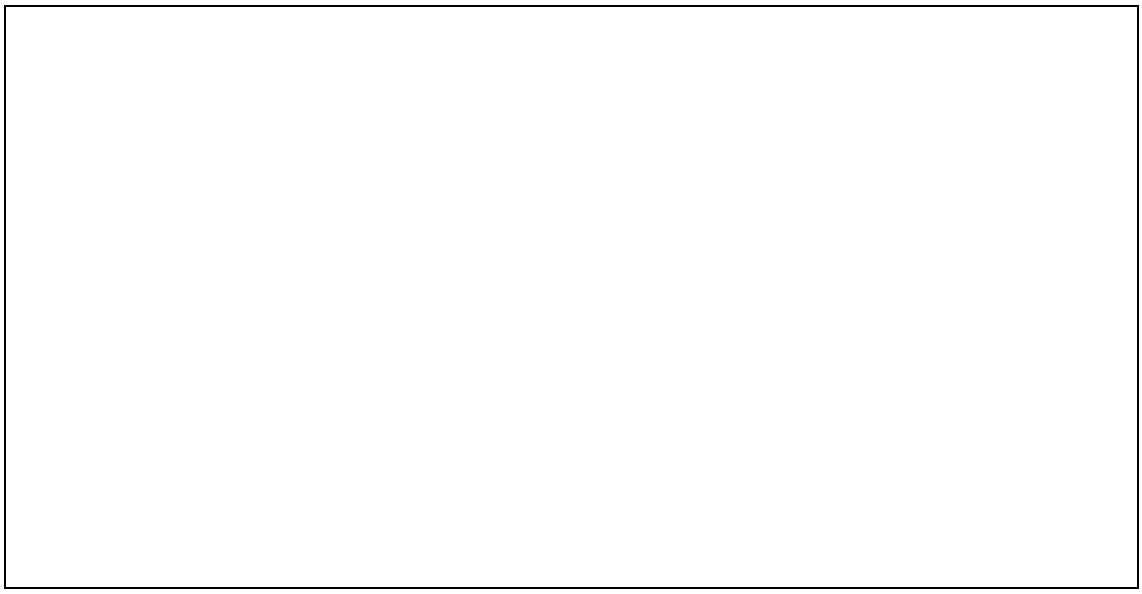

Figure 17. Optical images of the experimental set-up for field emission and the observed light during field emission for a single multiwall nanotube (a) and a multiwall carbon nanotube film (b). Emitted light intensity and current density as a function of time for a MWNT film (c).

To investigate further this phenomenon, we analysed the spectra of the emitted light for single MWNTs. A typical spectrum is displayed in the inset of Fig. 18. No significant changes in the shape of the spectrum were observed when the current was varied apart from a small shift (<25 meV) of the broad peak. The luminescence intensity I_p as a function of the emitted current I_e, as shown in Figure 14, followed a power law $I_p \sim I_e^{\alpha}$ with $\alpha=1.4\pm0.2$ in this case.

Figure 18. Variation of the total emitted intensity as a function of emitted current. The solid line is a power law fit of the experimental data, and yields an exponent of 1.4±0.2. Inset: spectra of field emission induced luminescence for one MWNT at 20 μA emitted current

There has been one report of observed luminescence on opened nanotubes[31] but it was attributed to an incandescence of carbon chains at the tip of the tube provoked by resistive heating. Our results however strongly suggest that the light emission is directly coupled to the field emission. The narrowness of the luminescence lines and the very small shifts with varying emitted current show that we are not in presence of blackbody radiation or of current-induced heating effects, but that photons are emitted following transitions between well-defined energy levels. Actually, the dependence of I_p versus I_e can be reproduced by a simple two-level model[40], where the density of states at the nanotube tip is simplified to a two level system, with the main emitting level at energy E_1 below or just above the Fermi energy, and a deep level at $E_2 < E_1$. When an electron is emitted from the deep level, it is replaced either by an electron from the tube body, or by an electron from the main level which can provoke the emission of a photon. From the Fowler-Nordheim model, the transition probability D(E) can be evaluated for each level, and in the frame of our model, $I_e \sim D(E_1)$, $I_p \sim D(E_2)$. It appears that I_p varies as a power of I_e with an exponent that depends on the separation of the levels[35], and that amounts to 1.51-1.65 for the energies observed here (typically 1.8 eV). This compares well to the experimental observations. These observations point to the presence of energy levels, and thus of localised states, at the tip. We estimate that one emitted photon corresponds to at least 10^6 field emitted electrons. With localised states at the tip, the greatest part of the emitted current will arise from occupied states with a large local density of states located near the Fermi level. Other, more deeply located electronic levels may also contribute to the field emission. In this case, the emitted electron will be replaced either by an electron from the semi-metallic tube body with an energy comparable to the level energy, or by a tip electron from the main emitting state. Clearly, the second alternative may provoke the emission of a photon. Although the tunneling probability for electrons from deeper state is several orders of magnitude lower than for the main emitting state, it will be readily sufficient to cause the observed light intensities.

Field emission mechanism

The results presented above show that the large field amplification factor, arising from the small radius of curvature of the nanotube tips, is partly responsible for the good emission characteristics. It is however still unclear whether the sharpness of nanotubes is their only advantage over other emitters, or if other properties also influence the emission performances. Most authors conclude that carbon nanotubes are metallic emitters, essentially because the I-V characteristics seem to follow the Fowler-Nordheim law. Our results[32] show, however, systematic deviations from the Fowler-Nordheim model at high emitted currents, which point to the fact that nanotubes cannot be considered as usual metallic emitters. Further observations confirm this conclusion, and strongly suggest that the electrons are not emitted from a metallic continuum as in usual metallic emitters, but rather from well-defined energy levels of ~0.3 eV half-width corresponding to localised states at the tip. First, the energy spread of nanotubes is typically half that of metallic emitters (about 0.2 eV), and the shape of the energy distribution suggests that the electrons are emitted from narrow energy levels[28,30]. Second, the observation of luminescence coupled to the field emission indicates that several of these levels participate to the field emission. Although the greatest part of the emitted current comes from occupied states with a large density of states near the Fermi level, other, deeper levels also contribute to the field emission. In fact, theoretical calculations and STM measurements on SWNTs and MWNTs show that there is a distinctive difference in the electronic properties between the tip and the cylindrical part of the tube. For MWNTs, the tube body is essentially graphitic, whereas SWNTs display a characteristic DOS[41,42] that reflects their one-dimensional character. In contrast, the local density of states at the tip presents sharp localised states that are correlated to the presence of pentagons[43,44]. Interestingly, the FWHM of these states and their separation is readily compatible with our observations. We conclude that the greatest part of the emitted current comes from occupied

states just below the Fermi level. The position of these levels with respect to the Fermi level, which depends primly on the tip geometry[44] (i.e., tube chirality and diameter and the eventual presence of defects), would be, together with the tip radius, the major factor that determines the field emission properties of the tube. Indeed, only tubes with a band state just below or just over the Fermi level are good candidates for field emission. Finally, it is worth noting that the presence of such localised states influences greatly the emission behaviour. At and above room temperature, the bodys' of MWNTs behave essentially as graphitic cylinders. This means that the carrier density at the Fermi level is very low, i.e., on the order of $5x10^{18}$ cm^{-3}, which is 3 orders of magnitude less than for a metal. Simulations show that the local density of states at the tip reaches values at least 30 times higher than in the cylindrical part of the tube. The field emission current would be far lower without these localised states for a geometrically identical tip since it depends directly on this carrier density. The crystalline structure also strongly influences the position and intensity of the localised states, which could explain the superiority of closed over opened or disordered MWNTs. Another complementary explanation for this observation is that the coupling of the tip states to the metallic body is probably far better for closed MWNTs, leading to an increased electron supply and thus higher emitted current.

ACKNOWLEDGEMENT

The work is supported by the Swiss National Foundation for Scientific Research.

REFERENCES

1. J.-M. Bonard et al., *Adv. Mater.* **9**, 827 (1997).
2. D. Xu et al., *Appl. Phys. Lett.* **75**, 481 (1999).
3. M.M.J. Treacy, T.W. Ebbesen and J.M. Gibson. *Nature* **381**, 678 (1996).
4. E.W. Wong, P.E. Sheehan and C.M. Lieber. *Science* **277**, 1971 (1997).
5. A. Krishnan,. E. Dujardin, T.W. Ebbesen, P.N. Yianilos and M.M.J. Treacy. *Phys. Rev. B* **58** (20) 14013 (1998).
6. J.-P. Salvetat, G.A.D. Briggs, J.-M. Bonard, R. R. Basca, A.J. Kulik, T. Stöckli, N.A. Burnham and L. Forró. *Phys. Rev. Lett.* **82** (5) 944 (1999).
7. J.-P. Salvetat, A.J. Kulik, J.-M. Bonard, G.A.D. Briggs, T. Stöckli, K. Méténier, S. Bonnamy, F.Béguin, N.A. Burnham and L. Forró. *Adv. Mater.* **11** (2) 161 (1999).
8. P. Poncharal, Z.L. Wang, D. Ugarte and W.A. de Heer. *Science* **283**, 1513 (1999).
9. D.A. Walters, L.M. Ericson, M.J. Casavant, J. Liu, D.T. Colbert, K.A. Smith and R.E. Smalley. *Appl. Phys. Lett.* **74** (25) 3803 (1999).
10. L.S. Schadler, S.C. Giannaris and P.M. Ajayan. *Appl. Phys. Lett.* **73** (26) 3842 (1998).
11. A. Hamwi, H. Alvergnat, S. Bonnamy and F. Béguin. *Carbon* **35**, 723 (1997).
12. S. Pekker, J.-P. Salvetat, E. Jakab, J.-M. Bonnard and L. Forró. *Proc. IWEPNM (Science and Technology of Molecular Nanostructures) - Kirchberg, Austria* - in press (1999).
13. F. Beuneu, C. l'Huillier, J.-P. Salvetat, J.-M. Bonnard and L. Forró. *Phys. Rev. B* **59** (8) 5945 (1999).
14. K. Hernadi, A. Fonseca, J.B. Nagy and D. Bernaerts. Catalytic synthesis of carbon nanotubes p. 81 - 97 in: *Supercarbon : Synthesis, Properties and Applications*. S. Yoshimura and R.P.H. Chang, Eds., Springer-Verlag, Berlin (1998).
15. O.Lourie, D.M. Cox and H.D. Wagner. *Phys. Rev. Lett.* 81 (8) 1638 (1998).
16. S.J. Tans *et al*., Nature 393, 49 (1998); see also: P.L. McEuen *ibid*., 15; R. *Martel et al.*, Appl. Phys. Lett. 73, 2447 (1998).
17. R. Saito *et al.,* Appl. Phys. Lett. 60, 2204 (1992); J. W. Mintmire *et al., Phys. Rev. Lett*. 68, 631 (1992).
18. D. Jerome and H. Schulz, *Adv. in Physics* 31, 299 91982).
19. M. Bockrath, D. H. Cobden, J. Lu, A. G. Rinzler, R. Smalley, L. Balents, P. L. McEuen, *Nature* 397, 598 (1999).
20. R. S. Lee, H. J. Kim, J. E. Fischer, A. Thess, R. E. Smalley, *Nature* 388, 255 (1997).
21. Bachtold *et al., Appl. Phys. Lett.* 73, 274 (1998).
22. C. Schönenberger *et al.*, to appear in *Appl. Phys. A*.
23. A. Bachtold, et al., *Nature* 397, 673 (1999).

24. M.P.A. Fisher and L. Glazman, in *Mesoscopic Electron Transport*, L.L.Sohn, L.P. Kouwenhoven, and G. Schön, eds., NATO ASI, Series E: Applied Sciences 345 (Kluwer Academic, Dordrecht 1997); R. Egger and A. O. Gogolin, *Phys. Rev. Lett*. 79, 5082 (1997); C.\ Kane, *et al.*, *ibid.* 5086.
25. G. Wagoner, *Phys. Rev.* 118:647 (1960).
26. M. Kosaka, T. W. Ebbesen, H. Hiura, K. Tanigaki, *Chem. Phys. Lett*. 225:161 (1994).
27. F. Beuneu, C. L'Huillier, J. P. Salvetat, J.-M. Bonard, L. Forró, *Phys. Rev. B* 59:5945 (1999).
28. Y. Yafet, *Solid State Phys.* 14:1 (1963). R. J. Elliott, *Phys. Rev.* 96, 266 (1954).
29. S. Schultz, M. R. Shanabarger, P. M. Platzman, *Phys. Rev. Lett.* 19, 749 (1967).
30. W.A. de Heer, A. Châtelain, D. Ugarte: *Science* 270, 1179 (1995).
31. A.G. Rinzler, J.H. Hafner, P. Nikolaev, L. Lou, S.G. Kim, D. Tomanek, P. Nordlander, D.T. Colbert, R.E. Smalley: *Science* 269, 1550 (1995).
32. J.-M. Bonard, F. Maier, T. Stöckli, A. Chatelain, W.A. de Heer, J.-P. Salvetat, L. Forró: *Ultramicroscopy* 73, 7 (1998).
33. J.-M. Bonard, J.-P. Salvetat, T. Stöckli, L. Forró, A. Chatelain: *Appl. Phys. A*, in press (1999).
34. S. Fan, M.G. Chapline, N.R. Franklin, T.W. Tombler, A.M. Cassell, H. Dai: *Science* 283, 512 (1999).
35. M. Fransen: *Towards high brightness, monochromatic electron sources*, PhD thesis, Technical University Delft (1999).
36. S. Frank, P. Poncharal, Z.L. Wang, W.A. de Heer: *Science* 280, 1744 (1998).
37. V.V. Zhirnov, A.B. Voronin, E.I. Givargizov, A.L. Meshcheryakova, *Proceedings of the IEEE International Vacuum Microelectronics Conference*, IVMC 1995, 340 (1996).
38. W.Z. Li, S.S. Xie, L.X. Qian, B.H. Chang, B.S. Zou, W.Y. Zhou, R.A. Zhao, G. Wang: Science 274, 1701 (1996).
39. H. Kind, J.-M. Bonard, C. Emmenegger, L.-O. Nilsson, K. Hernadi, E. Maillard-Schaller, L. Schlapbach, L. Forró and K. Kern, submitted to Adv. Mater. (1999).
40. J.-M. Bonard, T. Stöckli, W.A. de Heer, A. Chatelain, J.-P. Salvetat, L. Forró: Phys. Rev. Lett. 81, 1441 (1998).
41. J.W.G. Wildoer, L.C. Venema, A.G. Rinzler, R.E. Smalley, C. Dekker: Nature 391, 59 (1998); T.W. Odom, J.-L. Huang, P. Kim, C. M. Lieber: Nature 391, 62 (1998).
42. P. Kim, T.W. Odom, J.-L. Huang, C.M. Lieber: Phys. Rev. Lett. 82, 1225 (1999).
43. A. De Vita, J.-C. Charlier, X. Blase, R. Car: Appl. Phys. A. 68, 283 (1999).
44. D.L. Carroll, P. Redlich, P.M. Ajayan, J.-C. Charlier, X. Blase, A. De Vita, R. Car: Phys. Rev. Lett. 78, 2811 (1997).